

Eigenmode decomposition of the near-field enhancement in localized surface plasmon resonances of metallic nanoparticles

Titus Sandu¹

¹*National Institute for Research and Development in Microtechnologies,
126A, Erou Iancu Nicolae street, 077190, Bucharest, ROMANIA**

Abstract

I present a direct and intuitive eigenmode method that evaluates the near-field enhancement around the surface of metallic nanoparticles of arbitrary shape. The method is based on the boundary integral equation in the electrostatic limit. Besides the nanoparticle polarizability and the far-field response, the near-field enhancement around nanoparticles can be also conveniently expressed as an eigenmode sum of resonant terms. Moreover, the spatial configuration of the near-field enhancement depends explicitly on the eigenfunctions of both the BIE integral operator and of its adjoint. It is also established a direct physical meaning of the two types of eigenfunctions. While it is well known that the eigenfunctions of the BIE operator are electric charge modes, it is less known and used that the eigenfunctions of the adjoint represent the electric potential generated by the charge modes. For the enhanced spectroscopies the present method allows an easy identification of hot spots which are located in the regions with maximum charge densities and/or regions with fast variations of the electric potential generated by the charge modes on the surface. This study also clarifies the similarities and the differences between the far-field and the near-field behavior of plasmonic systems. Finally, the analysis of concrete examples like the nearly touching dimer, the prolate spheroid, and the nanorod illustrate some modalities to improve the near-field enhancement.

PACS numbers: 41.20.Cv, 71.45.Gm, 73.20.Mf

I. INTRODUCTION

The interaction of light with conduction electrons in metallic nanoparticles (NPs) results in localized surface plasmon resonances (LSPRs) that have the ability to guide, manipulate, and enhance light fields¹. The LSPRs are typically confined to length scales much smaller than the diffraction limit, which makes them suitable for localization and enhancement of electromagnetic fields. These properties enable applications in sensing², waveguiding³, optical information processing⁴, or photovoltaics⁵. Particularly, the near-field enhancement is exploited in near-field microscopy⁶, photoluminescence⁷, higher harmonic generation^{8,9}, and in several enhanced spectroscopies like enhanced fluorescence spectroscopy¹⁰, surface enhanced Raman spectroscopy (SERS)¹¹⁻¹³, and surface enhanced Infrared spectroscopy (SEIRS)¹⁴⁻¹⁶.

Numerical and theoretical methods used to predict and calculate the properties of LSPRs are successfully based on the integration of Maxwell's equations. The finite-difference time domain method¹⁷, the discrete-dipole approximation¹⁸, and the boundary element method^{19,20} are typical computational methods for full electromagnetic calculations of the optical response in metallic NPs. These complex numerical schemes present, however, little intuitive help about the nature and the physics of the LSPRs with respect to parameters like the shape (geometry) or complex dielectric functions of nanoparticles. The hybridization model has been proposed as an alternative approach which works very well in the quasi-static limit²¹. This model offers an intuitive physical picture in terms of plasmon eigenmodes. On the other hand, in the quasi-static limit, the LSPRs are in fact electrostatic resonances of a linear response operator²², which is defined on the boundary of the NP resulting a boundary integral equation (BIE) for an arbitrary geometry. This linear response operator and its adjoint, the Neumann-Poincare operator, are associated with the Neumann and Dirichlet problems in potential theory, respectively^{23,24}. In essence, the BIE method relates the LSPRs to the eigenmodes of the linear response operator and the Neumann-Poincare operator, such that the spectral studies of the linear response operator provide useful information about the LSPRs. The BIE method may work perturbatively even beyond the quasistatic limit^{25,26}. Moreover, being able to calculate the polarizability of a generic dielectric particle, the method can be applied not only to LSPRs in metallic NPs, but also for polarizability calculations of biological cells in radiofrequency²⁷. Like the hybridization model, the spec-

tral approach to BIE offers the same advantages of intuitive view of plasmon eigenmodes. The method can be extended to clusters of NPs²⁸ such that symmetry and selection rules that are used in the hybridization model²⁹ can be applied directly in BIE^{30,31} by considering the cluster eigenmodes as hybridizations of individual NP eigenmodes³².

Factors like composition, size, geometry, as well as the embedding media determine the LSPRs of metallic NP³³. In many applications there is a need for precise locations of the LSPRs. In SEIRS applications, for example, the spectral localization of the LSPR needs to be as close as possible to the molecular vibration that is to be enhanced and therefore sensed. In addition to that, the near-field enhancement factor is a key figure of merit in the enhanced spectroscopies where the geometry plays an important role. Large near-field enhancement occurs at a sharp tip by the lightning-rod effect³⁴ or at the junctions of NP dimers³⁵. The geometrical arrangement in dimers, as opposed to single NPs, exhibit much stronger field enhancements; thus, as the distance between dimer NPs decreases, the near-field enhancement increases in the space between the NPs of the dimer^{35–38}.

While the BIE method permits the calculation of near-field enhancement³⁹ a direct and intuitive way to extract the near-field enhancement factor is still needed. In this work I present a method that provides explicitly the near-field enhancement and its spatial variation in terms of eigenfunctions of the linear response operator and its adjoint. The spatial distribution of the field enhancement normal to the surface of the NP is proportional to the eigenfunctions of the linear operator. These eigenfunctions are charge modes, therefore the near-field maxima occur at the maxima of the surface charge density. On the other hand, the tangential component of the near-field enhancement is proportional to the derivative of the adjoint operator eigenfunctions, which are, in fact, the surface electric potential generated by the charge modes. The latter aspect has been hardly used in plasmonic applications. In addition to that, the current method directly ascertains the relationship between far-field and near-field spectral properties of the LSPRs⁴⁰. The proposed method has also limitations. First, it is valid only in the quasistatic approximation, hence the NPs must be much smaller than the light wavelength. The second issue comes from the quantum nature of the LSPR phenomenon. Thus the electron spill-out and the nonlocality of the electron interaction determine a different electric field behavior at the surface of the NP^{41–44}. However, at distances above 1 nm the classical description works well. It is proved by several examples that, despite these shortcomings, the present method remains a powerful tool for locating

and improving the near-field enhancement in plasmonic systems.

The paper has the following structure. The next section details exhaustively the method of calculating the spatial configuration of the near-field enhancement as depending on the eigenvalues and eigenfunctions of the BIE operators. Section III presents the numerical implementation and two comparative studies: the sphere versus the nearly touching dimer and the nanorod versus the prolate spheroid. In the last section I summarize the conclusions.

II. THEORETICAL BACKGROUND

For the sake of clarity I present first the main results of the spectral approach to the BIE method. Let us consider a NP of volume V which is delimited by the surface Σ and has a dielectric permittivity $\epsilon_1(\omega)$. The NP is embedded in a uniform medium of permittivity $\epsilon_0(\omega)$. In the quasi-static limit, i. e., the size of NP is much smaller than the wavelength of incident radiation, the applied field is almost homogeneous and the Laplace equation suffices to describe the behavior of the NP under the incidence of the light

$$\Delta\Phi(\mathbf{x}) = \mathbf{0}, \quad \mathbf{x} \in \mathfrak{R}^3 \setminus \Sigma, \quad (1)$$

where Φ is the potential of the total electric field \mathbf{E}_{total} , i.e., $\mathbf{E}_{total}(\mathbf{x}) = -\nabla\Phi(\mathbf{x}) = \mathbf{E}(\mathbf{x}) + \mathbf{E}_0(\mathbf{x})$ and \mathfrak{R}^3 is the Euclidian 3-dimensional space in which the NP of surface Σ is embedded. The boundary conditions are: $\epsilon_0(\omega)\frac{\partial\Phi}{\partial\mathbf{n}}|_+ = \epsilon_1(\omega)\frac{\partial\Phi}{\partial\mathbf{n}}|_-$ for $\mathbf{x} \in \Sigma$; and $-\nabla\Phi(\mathbf{x}) \rightarrow \mathbf{E}_0$ for $|\mathbf{x}| \rightarrow \infty$, where \mathbf{n} is the outer normal to the surface Σ and \mathbf{E}_0 is the incident (applied) field. The solution of (1) can be expressed as a superposition of the applied electric potential $-\mathbf{x} \cdot \mathbf{E}_0$ and a single-layer potential generated by the surface charge distribution $u(\mathbf{x})$,

$$\Phi(\mathbf{x}) = -\mathbf{x} \cdot \mathbf{E}_0 + \frac{1}{4\pi} \int_{\mathbf{y} \in \Sigma} \frac{u(\mathbf{y})}{|\mathbf{x} - \mathbf{y}|} d\Sigma_{\mathbf{y}}. \quad (2)$$

The single layer-potential utilized in (2) can define on Σ a symmetric operator \hat{S} that acts on the Hilbert space $L^2(\Sigma)$ of square-integrable functions on Σ as

$$\hat{S}[u] = \frac{1}{4\pi} \int_{\mathbf{y} \in \Sigma, \mathbf{x} \in \Sigma} \frac{u(\mathbf{y})}{|\mathbf{x} - \mathbf{y}|} d\Sigma_{\mathbf{y}}. \quad (3)$$

In the Hilbert space $L^2(\Sigma)$, the scalar product of two functions $\tilde{u}_1(\mathbf{x})$ and $\tilde{u}_2(\mathbf{x})$ is defined as

$$\langle \tilde{u}_1 | \tilde{u}_2 \rangle = \int_{\mathbf{x} \in \Sigma} \tilde{u}_1^*(\mathbf{x}) \tilde{u}_2(\mathbf{x}) d\Sigma_x. \quad (4)$$

The derivative of the single-layer potential presents discontinuities across the boundary Σ . This can be used to rewrite (1) with the help of the operator also defined on $L^2(\Sigma)$ ^{23,24,27}

$$\hat{M}[u] = \frac{1}{4\pi} \int_{\mathbf{y} \in \Sigma, \mathbf{x} \in \Sigma} \frac{u(\mathbf{y}) \mathbf{n}_x \cdot (\mathbf{x} - \mathbf{y})}{|\mathbf{x} - \mathbf{y}|^3} d\Sigma_y. \quad (5)$$

Then, the equation fulfilled by the charge distribution $u(\mathbf{x})$ in Eq. (2) has the following operator form

$$\frac{1}{2\lambda} u(\mathbf{x}) - \hat{M}[u] = \mathbf{n} \cdot \mathbf{E}_0, \quad (6)$$

with $\lambda = \frac{\epsilon_1 - \epsilon_0}{\epsilon_1 + \epsilon_0}$. The function $u(\mathbf{x})$, which defines through (2) the solution of (1), can be found by the knowledge of the eigenvalues χ_k and eigenfunctions of \hat{M} and its of adjoint operator expressed as:

$$\hat{M}^\dagger[v] = \frac{1}{4\pi} \int_{\mathbf{y} \in \Sigma, \mathbf{x} \in \Sigma} \frac{v(\mathbf{y}) \mathbf{n}_y \cdot (\mathbf{x} - \mathbf{y})}{|\mathbf{x} - \mathbf{y}|^3} d\Sigma_y. \quad (7)$$

This is the Neumann-Poincare operator²⁴ and has the physical significance of an electric potential generated by a dipole distribution on Σ . The operators \hat{M} and \hat{M}^\dagger have several general properties. Their eigenvalues are equal and restricted to $[-1/2, 1/2]$, while their eigenfunctions are bi-orthogonal, i.e. if $\hat{M}[u_i] = \chi_i u_i$ and $\hat{M}^\dagger[v_j] = \chi_j v_j$, then $\langle v_j | u_i \rangle = \delta_{ij}$ ^{22,25,27,45,46}. However, the eigenfunctions u_i and v_i are coupled through the Plemelj's symmetrization principle²⁴

$$\hat{M}^\dagger \hat{S} = \hat{S} \hat{M}. \quad (8)$$

One can notice that the operator \hat{M} can be made symmetric with respect to the metric defined by the symmetric and non-negative operator \hat{S} , i. e., for any $\tilde{u}_1, \tilde{u}_2 \in L^2(\Sigma)$: $\langle \tilde{u}_1 | \tilde{u}_2 \rangle_S = \langle \tilde{u}_1 | \hat{S}[\tilde{u}_2] \rangle$. Using (8) and the norm defined by \hat{S} one can relate the eigenfunctions u_i and v_i by

$$v_i = \hat{S}[u_i]. \quad (9)$$

From physical point of view, Eq. (9) denotes that v_i is the electric potential generated on surface Σ by the charge distribution u_i and, to the author's knowledge, Eq. (9) has not been used in plasmonic applications. As it will be shown later, Eq. (9) is instrumental for the calculation of the near-field enhancement in a coordinate system directly related to the geometry of the NP.

The explicit solution of (6) can be expressed in terms of eigenvalues and eigenfunctions of \hat{M} and \hat{M}^\dagger as^{27,46}

$$u = \sum_k \frac{n_k}{\frac{1}{2\lambda} - \chi_k} u_k. \quad (10)$$

In (10) $n_k = \langle v_k | \mathbf{n} \cdot \mathbf{N} \rangle$, where \mathbf{N} the unit vector of the applied field given by $\mathbf{E}_0 = E_0 \mathbf{N}$. The term n_k is the contribution of the k^{th} eigenmode to the solution of (6) and, as shown below, it represents the weight coefficient of the k^{th} eigenmode to the evanescent near-field. Also, the charge density u determines an electric potential v on Σ via Eq. (9). In addition, (10) has one part that depends on the geometry through the eigenfunctions and the second part that depends on both the geometry (through the eigenvalues) and the dielectric properties.

The charge density u determines the volume-normalized polarizability of the NP as the volume-normalized dipole moment generated by u along the applied field direction^{27,46}

$$\alpha = \sum_k \frac{w_k}{\frac{1}{2\lambda} - \chi_k}, \quad (11)$$

where $w_k = n_k \langle \mathbf{r} \cdot \mathbf{N} | u_k \rangle / V$ is the weight of the k^{th} eigenmode to the NP polarizability and \mathbf{r} is the position vector that determines Σ . The parameter $w_k < 1$ is scale-invariant and solely determined by the geometry of the NP.

One may obtain explicit expressions for α if a Drude form $\epsilon = \epsilon_m - \omega_p^2 / (\omega(\omega + i\gamma))$ is used for the complex permittivity of metals. Here, ϵ_m incorporates the interband transitions (with little variations in VIS-IR) and the term ϵ_∞ . The parameter ω_p is the plasma resonance frequency of free electrons and γ is the Drude relaxation term. Dielectrics are in contrast described by a real and constant dielectric function $\epsilon = \epsilon_d$. Including these explicit expressions for the dielectric permittivities, the NP polarizability is⁴⁶

$$\alpha_{plas}(\omega) = \sum_k \frac{w_k(\varepsilon_m - \varepsilon_d)}{\varepsilon_{eff,k}} - \frac{w_k}{1/2 - \chi_k} \frac{\varepsilon_d}{\varepsilon_{eff,k}} \frac{\tilde{\omega}_{pk}^2}{\omega(\omega + i\gamma) - \tilde{\omega}_{pk}^2}, \quad (12)$$

where $\tilde{\omega}_{pk}^2 = (1/2 - \chi_k)\omega_p^2/\varepsilon_{eff,k}$ is the square of a frequency associated with the resonance of the k^{th} eigenmode and $\varepsilon_{eff,k} = (1/2 + \chi_k)\varepsilon_d + (1/2 - \chi_k)\varepsilon_m$ is an effective dielectric parameter. In visible and infrared Eq. (12) has a slow-varying part and a sum of fast-varying Drude-Lorentz terms $-w_k/(1/2 - \chi_k) \times \varepsilon_d/\varepsilon_{eff,k} \times \tilde{\omega}_{pk}^2/(\omega(\omega + i\gamma) - \tilde{\omega}_{pk}^2)$.

The far-field behavior of the interaction of electromagnetic fields with metallic NPs is determined by the induced dipole that is proportional to the normalized polarizability α . The imaginary part of the polarizability is directly related to the absorption/extinction of light which is the far-field effect of the LSPRs. Thus the cross-section of the extinction is¹

$$C_{ext} = \frac{2\pi}{\lambda} Im(\alpha_{plas}V), \quad (13)$$

where λ is the wavelength of the incident radiation. Now it becomes apparent that w_k signifies the weight of the k^{th} eigenmode to the far-field of the LSPRs. The eigenmodes which have $w_k \neq 0$ couple with light and therefore are bright eigenmodes, whilst those which have $w_k = 0$ are dark eigenmodes. The eigenmode with the largest eigenvalue $1/2$ is dark because always $\langle v_1 | \mathbf{n} \cdot \mathbf{N} \rangle = 0$. Physically, it represents a monopole charge distribution. The strength of each bright eigenmode is in fact proportional to the geometric factor $w_k/(1/2 - \chi_k)$, such that some eigenvalues χ_k close to $1/2$ might show strong plasmon resonance response even though w_k may have low values⁴⁶. Moreover, as it will be seen below, if one neglects γ , then the resonance frequency $\tilde{\omega}_{pk}$ is just the LSPR frequency of the k^{th} eigenmode. Therefore, larger χ_k 's mean longer plasmon wavelengths and, as an eigenvalue χ_k approaches $1/2$, the plasmon resonance frequency moves in the mid-infrared^{38,46}.

In principle, the near-field around NP can be evaluated from Eq. (10) by calculating first the electric potential and then the electric field. Below I will present compact and intuitive relations for the near-field at the surface Σ of the NP. These relations allow a decomposition of the near-field at Σ in normal and tangent components and a direct calculation of the near-field enhancement. For this purpose I will utilize a coordinate system directly related to the parameterization of surface Σ . Let us suppose that Σ is locally parametrized by $x = X(\xi^1, \xi^2)$, $y = Y(\xi^1, \xi^2)$, and $z = Z(\xi^1, \xi^2)$, where ξ^1, ξ^2 are the independent parameters defining Σ . If the functions X, Y , and Z are sufficiently smooth, the vectors tangent to Σ

are defined by⁴⁷

$$\mathbf{r}_{\xi^{1,2}} = \frac{\partial \mathbf{r}}{\partial \xi^{1,2}}, \quad (14)$$

whose norms $h_{\xi^{1,2}} = |\mathbf{r}_{\xi^{1,2}}|$ are the Lamé coefficients. The unit vectors $\mathbf{t}_{\xi^{1,2}} = \mathbf{r}_{\xi^{1,2}}/h_{\xi^{1,2}}$ determine the normal on Σ as the cross-product

$$\mathbf{n} = \mathbf{t}_{\xi^1} \times \mathbf{t}_{\xi^2} / |\mathbf{t}_{\xi^1} \times \mathbf{t}_{\xi^2}|. \quad (15)$$

In Eqs. (14) and (15) the position vector \mathbf{r} designates a point on Σ and therefore depends on ξ^1 and ξ^2 . The following nonlinear coordinate transformation $(x, y, z) \leftrightarrow (\xi^1, \xi^2, \xi^3)$ allows the decomposition of the induced electric field on Σ in components along the normal and in the tangent plane. The transformation is given by $x = X(\xi^1, \xi^2) + \xi^3 n_x(\xi^1, \xi^2)$, $y = Y(\xi^1, \xi^2) + \xi^3 n_y(\xi^1, \xi^2)$, and $z = Z(\xi^1, \xi^2) + \xi^3 n_z(\xi^1, \xi^2)$, where n_x, n_y, n_z are, respectively, the x -, y -, z -components of the normal \mathbf{n} . Thus the induced electric field on Σ is actually calculated in the neighborhood of $\xi^3 = 0$. The vectors $(\mathbf{r}_{\xi^1}, \mathbf{r}_{\xi^2}, \mathbf{n})$ make a basis and a three-frame generated by the above nonlinear coordinate transformation. The basis $(\mathbf{r}^{\xi^1}, \mathbf{r}^{\xi^2}, \mathbf{n})$ that is dual to $(\mathbf{r}_{\xi^1}, \mathbf{r}_{\xi^2}, \mathbf{n})$ is given by

$$\mathbf{r}^{\xi^1} = \frac{\mathbf{r}_{\xi^2} \times \mathbf{n}}{\mathbf{n} \cdot (\mathbf{r}_{\xi^1} \times \mathbf{r}_{\xi^2})}, \quad (16)$$

$$\mathbf{r}^{\xi^2} = \frac{\mathbf{n} \times \mathbf{r}_{\xi^1}}{\mathbf{n} \cdot (\mathbf{r}_{\xi^1} \times \mathbf{r}_{\xi^2})}. \quad (17)$$

Then on Σ the induced electric field along the normal \mathbf{n} is given with the help of \hat{M} as²⁴

$$\tilde{E}_n(\xi^1, \xi^2) = (\hat{M} + 1/2)u = \sum_k \frac{n_k(\chi_k + 1/2)}{\frac{1}{2\lambda} - \chi_k} u_k(\xi^1, \xi^2). \quad (18)$$

From Eqs. (9) and (10) and from the expression of the gradient in the general curvilinear coordinates,⁴⁷ the rest of the induced electric field laying onto the tangent plane to Σ has the following expression

$$\begin{aligned} \tilde{\mathbf{E}}_t(\xi^1, \xi^2) &= -\nabla_t v(\xi^1, \xi^2) \\ &= -\sum_k \frac{n_k}{\frac{1}{2\lambda} - \chi_k} \left[\frac{\partial v_k(\xi^1, \xi^2)}{\partial \xi^1} \mathbf{r}^{\xi^1} + \frac{\partial v_k(\xi^1, \xi^2)}{\partial \xi^2} \mathbf{r}^{\xi^2} \right]. \end{aligned} \quad (19)$$

When the three-frame $(\mathbf{r}_{\xi^1}, \mathbf{r}_{\xi^2}, \mathbf{n})$ is orthogonal, the induced field tangent to Σ takes the form

$$\begin{aligned} \tilde{\mathbf{E}}_t(\xi^1, \xi^2) = & \\ & - \sum_k \frac{n_k}{\frac{1}{2\lambda} - \chi_k} \left[\frac{1}{h_{\xi^1}} \frac{\partial v_k(\xi^1, \xi^2)}{\partial \xi^1} \mathbf{t}_{\xi^1} + \frac{1}{h_{\xi^2}} \frac{\partial v_k(\xi^1, \xi^2)}{\partial \xi^2} \mathbf{t}_{\xi^2} \right]. \end{aligned} \quad (20)$$

Equations (18) and (19) are the main results of this work. These equations provide an eigenmode decomposition of the near-field and an intuitive and a direct relationship between the LSPRs and their local field enhancements. In the vicinity of Σ the total near-field is the sum of the induced electric field $\tilde{\mathbf{E}}$ and the applied field \mathbf{E}_0 : $\tilde{\mathbf{E}}_{total} = \tilde{\mathbf{E}} + \mathbf{E}_0 = \tilde{\mathbf{E}}_t + \tilde{E}_n \mathbf{n} + \mathbf{E}_0$. The total electric field is a complex-valued quantity. Its modulus represents the strength of the total electric field and its phase is the phase shift between the applied and the total field.

The near-field enhancement is

$$\frac{|\tilde{\mathbf{E}}_{total}|}{|\mathbf{E}_0|} \cong \frac{|\tilde{\mathbf{E}}|}{|\mathbf{E}_0|} \quad (21)$$

since $|\tilde{\mathbf{E}}|/|\mathbf{E}_0| \gg 1$ at the plasmon resonance frequency. There are several consequences of these results. First, the equations (18) and (19) locate the hot spots of the near-field enhancement. The spatial maxima of the normal component of the near-field enhancement are provided by the maxima of the absolute value of u_k , whilst the maxima of the tangent component are localized in the regions of fast variations of v_k . Although v_k is a smooth version of u_k by (9), the areas with fast variations of v_k may come from the regions of rapid change of u_k . Thus the simple inspection of the eigenfunctions indicates the regions with high near-field enhancement. Second, although there is a direct relation between the near- and far-field coupling to the electromagnetic radiation via $w_k = n_k \langle \mathbf{x} \cdot \mathbf{N} | u_k / V$, there are eigenmodes with large near-field enhancements but with small dipole moments, thus being almost dark in the far-field. Third, in the Drude metal case, Eqs. (18) and (19) have a frequency-dependence form similar to Eq. (12). Starting from the latter one can arrive at a fourth consequence related to the difference between the near- and far-field spectral properties. Recent works indicate a spectral shift between the maxima of the far- and near-field spectral response^{40,48,49}. From eqs. (12) and (13) the far-field spectral maximum of the k^{th} LSPR is the maximum of the function

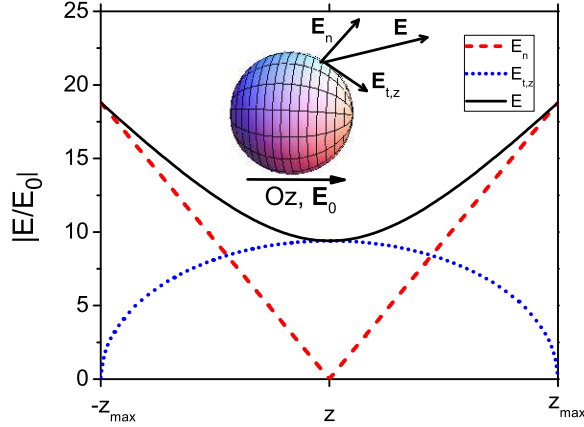


FIG. 1: Spatial dependence of the near-field enhancement components for a metallic nanosphere in the $x-z$ plane at the resonance frequency. Normal component-red dashed line, tangent component-blue dotted line, total near-field enhancement-black solid line). All three quantities are axially symmetric about z -axis. The inset shows a nanosphere and the directions of the applied and induced fields.

$$Im(\alpha_{plas}) \propto \frac{w_k}{1/2 - \chi_k} \frac{\varepsilon_d}{\varepsilon_{eff,k}} \frac{\tilde{\omega}_{pk}^2 \omega^2}{(\omega^2 - \tilde{\omega}_{pk}^2)^2 + (\omega\gamma)^2}, \quad (22)$$

whose maximum is at $\omega = \tilde{\omega}_{pk}$. On the other hand, if it is assumed that the k^{th} LSPR is well resolved then the spectral maximum of the k^{th} LSPR near-field is the maximum of

$$|\mathbf{E}| \propto \frac{n_k}{1/2 - \chi_k} \frac{\varepsilon_d}{\varepsilon_{eff,k}} \tilde{\omega}_{pk}^2 \frac{1}{\sqrt{(\omega^2 - \tilde{\omega}_{pk}^2)^2 + (\omega\gamma)^2}}. \quad (23)$$

The maximum of (23) is at $\omega = \sqrt{\tilde{\omega}_{pk}^2 - \gamma^2/2}$. The results provided by (22) and (23) explain in a general fashion the spectral shift between the far- and near-field without invoking a mechanical analogy of the plasmon resonance phenomenon⁴⁰. Nanoparticles made of metals with larger damping constants γ show larger and easier discernible shifts⁵⁰. In the next section I am going to analyze two numerical examples that show the utility of the BIE method in estimating the near-field enhancement.

III. NUMERICAL EXAMPLES

In the numerical implementation of the method presented above I consider NP shapes with axial symmetry. The surface Σ may be parameterized by equations like $\{x, y, z\} = \{g(z) \cos \phi, g(z) \sin \phi, z\}$ or $\{x, y, z\} = \{r(\theta) \sin \theta \cos \phi, r(\theta) \sin \theta \sin \phi, r(\theta) \cos \theta\}$, where $g(z)$ and $r(\theta)$ are smooth and arbitrary functions of z and θ , respectively. In the first case the independent parameters are z and ϕ , while in the second case the parameters are θ and ϕ . These two parameterizations provide an orthogonal three-frame on Σ and a smooth mapping to a standard sphere. Hence the basis functions in which the operators \hat{M} , \hat{M}^\dagger , and \hat{S} are expressed are easily related to spherical harmonics Y_{lm} ^{27,46}. The axial symmetry ensures some selection rules of the LSPRs. Thus for field polarization parallel to the symmetry axis the selection rules imply basis functions with $m = 0$. In the same time, for a transverse polarization only the basis functions with $m = 1$ give non-zero matrix elements. Numerical calculations are made with gold NPs immersed in water with a dielectric constant $\varepsilon_d = 1.7689$. The dielectric function of the gold NPs is adjusted such that the plasmon resonance wavelength of a gold nanosphere immersed in water is at 529 nm. The following Drude constants are used for gold: $\varepsilon_m = 11.2$, $\hbar\omega_p = 9$ eV, and $\hbar\gamma = 100$ meV. The damping constant γ incorporates the bulk damping and the damping due to surface collisions of electrons⁴⁶.

A. Metallic nanosphere and spherical dimer in parallel field

The dimers exhibit large near-field enhancement³⁵⁻³⁷ and, in particular, the nearly touching dimers reveal also a resonance in infrared part of the spectrum^{38,46}. In this subsection I examine and compare the plasmon resonance properties of spherical NPs and of nearly touching dimers made of almost spherical particles. Although a nearly touching dimer proves to be difficult to fabricate, it may model a system closely related to those that have large SERS enhancement like the nanostars deposited onto a smooth gold surface¹³. A sphere presenting a tip close to a gold film and showing a large near-field enhancement⁵¹ may have a correspondent in a nearly touching dimer due to the image charge that appears like another particle supporting LSPRs⁵².

The sphere surface can be described by the equation $\{x, y, z\} = \{g(z) \cos \phi, g(z) \sin \phi, z\}$,

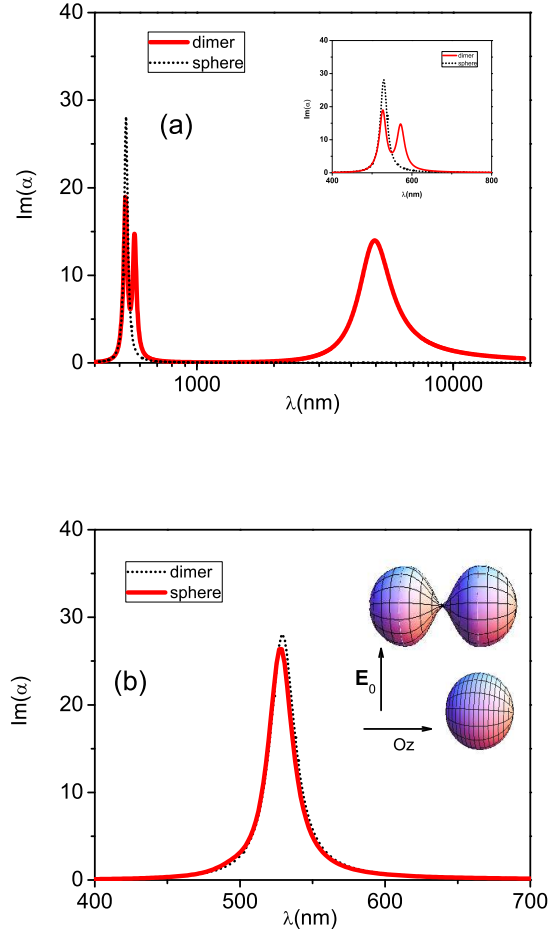


FIG. 2: Imaginary part of polarizability for a gold nanosphere (black dotted line) and for a dimer of nearly spherical NPs (red full line) in (a) visible and infrared for an applied field parallel to z -axis and in (b) visible for the polarization perpendicular to z -axis. The scaling of the polarizability by the NP volume makes it a dimensionless quantity. The inset of (a) shows the imaginary part of polarizability only in visible and the inset of (b) shows the shapes of the nanosphere and the dimer.

where $g(z) = z_{max} \sqrt{1 - z^2/z_{max}^2}$ and z_{max} is the radius of the sphere. The shape of a dimer made of nearly spherical particles connected by a tight junction is taken from a more general equation for clusters of n touching particles having the same parametrization $\{x, y, z\} = \{g(z) \cos \phi, g(z) \sin \phi, z\}$, where⁴⁶

$$g(z) = A(1 + S(z)S(z) - (n - 1)a) \times \frac{\sqrt{1 - ((z - S(z)(n - 1)a)/a)^2}}{1 + (1 + b(z - S(z)(n - 1)a)^2)^2} [1 - Fl(\frac{S(z)z + a}{na})] \times \left[h + 2(A - h)(1 - \frac{1}{1 + (1 - (H(z)/a)^2)^2}) \right]$$

with $H(z) = Mod((-1)^{Fl(z/a)+n-1}z, a)$; $S(z)$ is signum function and equals -1, 0 or 1 if z is negative, zero or positive; $Fl(z)$ is the greatest integer less than z ; and $Mod(x, y)$ is the remainder of the division of x by y . Parameters A and a define the radius of the maximum cross-section and the half-length of any particle in the cluster, respectively. Thus the ratio a/A is the aspect ratio of a particle in the cluster. Parameter b determines the curvature of the end caps such that for spherical end caps $b = 0$ - while h gives the cross-section size of the connecting gap. For a nearly spherical dimer $n = 2$, $a = A = z_{max}$, $b = 0$, and $h = 0.025z_{max}$.

The first example examined is the nanosphere, whose field enhancement is a textbook calculation¹. The near-field enhancement of a nanosphere in the $x - z$ plane at resonance frequency is presented in Fig. 1. In the $x - z$ plane the x -coordinate is determined by the equation $x = h(z)$. The field polarization is parallel to z -axis, therefore the induced field is also symmetric about z -axis. A comparison of far-field spectra for the nanosphere and for the dimer is given in Fig. 2. The bright eigenmode is the dipole mode corresponding to the second largest eigenvalue $\chi_2 = 1/6$ with $w_2 = 1$ (see also Table I). Its corresponding eigenfunctions $u_2(z), v_2(z) \propto z$. Therefore in Fig. 1, the normal component of $|\mathbf{E}/\mathbf{E}_0|$ is linear in z , while the tangent component acquires the z -dependence of $1/h_z(z)$, where $h_z(z)$ is the Lamé coefficient for the independent parameter z . Along z -axis the maximum near-field enhancement is about 19 occurring at the north and south poles of the nanosphere.

In Table I there are presented the most representative eigenvalues of both the nanosphere and the dimer, while the far-field spectral behavior is plotted in Fig. 2. The comparative analysis of the far-field spectrum has revealed that, with respect to a single sphere, the dimer has two more LSPRs in addition to that corresponding to the nanosphere alone: one in visible at longer wavelengths and the other more displaced into mid-infrared⁴⁶. The eigenfunctions of the sphere and of the dimer are plotted in the Supplementary Information. The representative eigenmodes of the dimer are either hybrid modes of the nanosphere eigenmodes or

TABLE I: The most representative eigenvalues, their plasmon resonance wavelengths, and their weights w_k and n_k for a sphere and a dimer made of nearly spherical particles connected by a tight junction. The field is parallel ($\mathbf{E}_0 \parallel \mathbf{Oz}$ and $m = 0$) or perpendicular ($\mathbf{E}_0 \perp \mathbf{Oz}$ and $m = 1$) to symmetry axis.

sphere					dimer				
k	χ_k	$\lambda_k(\text{nm})$	w_k	n_k	k	χ_k	$\lambda_k(\text{nm})$	w_k	n_k
$m = 0$					$m = 0$				
1	0.5	∞	0.0	0.0	1	0.5	∞	0.0	0.0
					2	0.498571	4867	0.0071	-0.025
					3	0.272	571.6	0.287	-1.97
					4	0.201	540	0.0	0.0
2	0.167	529	1	-3.34	5	0.159	526.9	0.658	-3.66
					6	0.122	517.8	0.0	0.0
3	0.1	513	0.0	0.0	7	0.112	515.5	0.027	-0.79
					8	0.067	506.6	0.0	0.0
$m = 1$					$m = 1$				
1	0.167	529	1	-2.36	1	0.214	544.5	0.0	0.0
					2	0.162	527.8	0.96	-3.09
					3	-0.014	494.5	0.022	0.557
					4	-0.086	486.3	0.01	-0.408

proper eigenmodes of the dimer. Thus the first eigenmode of the nanosphere ($k = 1$) has two corresponding hybrid eigenmodes in the dimer ($k = 1$ and $k = 2$): one is a symmetric combination of the nanosphere eigenmodes and the other is an anti-symmetric combination. Only the anti-symmetric mode is a bright eigenmode. In general, if a sphere eigenmode is symmetric under the mirror symmetry $z \leftrightarrow -z$, an anti-symmetric hybridization leads to a bright eigenmode of the dimer. Conversely, if a sphere eigenmode is anti-symmetric under the mirror reflection $z \leftrightarrow -z$, a symmetric hybrid can couple with the light. Consequently, the fifth and the sixth dimer eigenmodes are the hybrids of the second sphere eigenmode and the third sphere eigenmode creates the seventh and the eighth dimer eigenmodes.

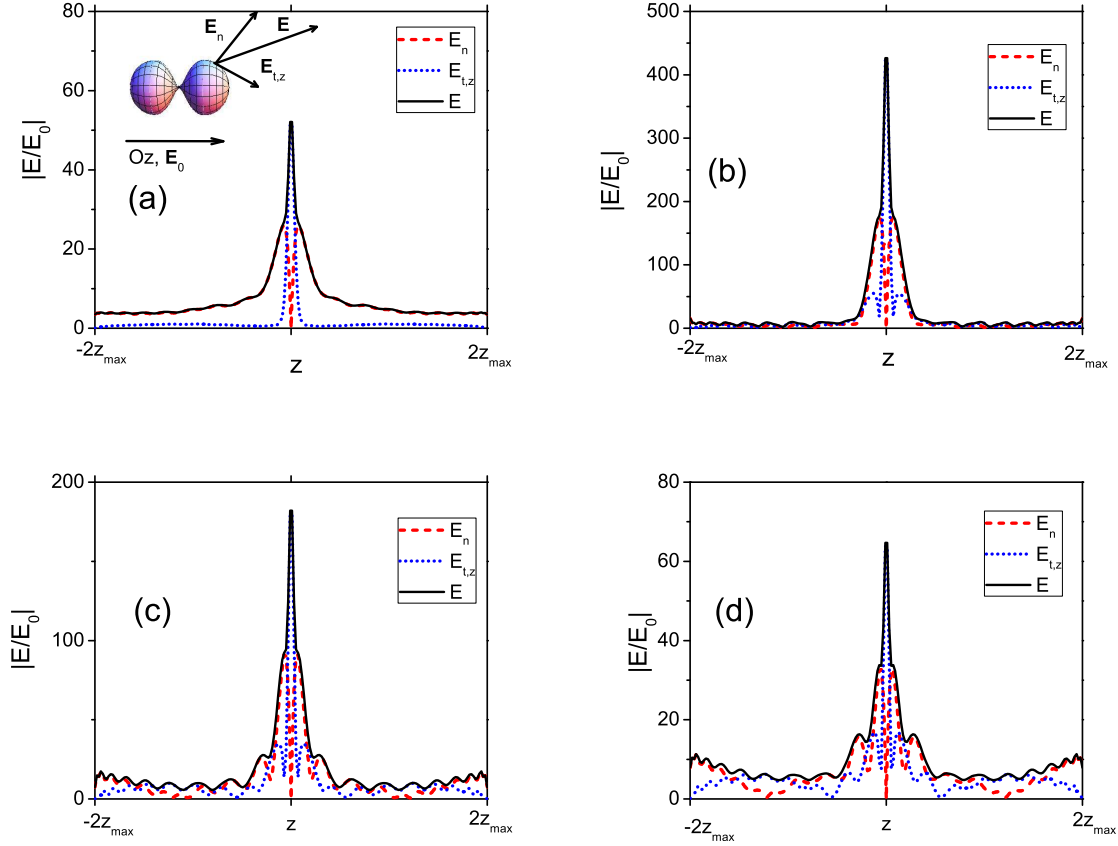


FIG. 3: The near-field enhancement in the $x - z$ plane at four plasmon resonance wavelengths given by: (a) the second ($\lambda = 4867$ nm), (b) the third ($\lambda = 571.6$ nm), (c) the fifth ($\lambda = 526.9$ nm), and (d) the seventh ($\lambda = 515.5$ nm) dimer eigenmode from Table I. The normal component of the enhancement is plotted by red dashed line, the tangent component by blue dotted line, and the total enhancement by black full line. The polarization of the field is parallel to the symmetry axis of the dimer, hence all three fields have axial symmetry. The inset of (a) shows the components of the near-field induced at the dimer surface.

The third and the fourth dimer eigenmodes are characteristic to dimer itself. From the Supplementary Information one can see that the third eigenmode exhibits just a large dipole at the junction and therefore is bright. This mode has been noticed in clusters of touching nanoparticles with $A/a \leq 1^{46}$. On the other hand, the fourth eigenmode has a large charge accumulation at the junction but is even with respect to the mirror symmetry $z \leftrightarrow -z$, being therefore dark. In the terminology of Refs. 53 and 54 the hybrid modes are "atomic" modes,

while the modes like the third and the fourth eigenmode are called "molecular" modes. On the whole, all bright eigenmodes manifest large charge accumulations and fast changes of electric potential at the junction. According to Eqs. (18) and (19) at the resonance wavelengths there are huge near-field enhancements around the junction of the dimer as depicted in Fig. 3. The enhancement is mostly provided by the normal component of the electric field, excepting the middle of the dimer, where the normal field vanishes and the tangent component contributes to the enhancement. The weights w_2 and n_2 of the second eigenmode are rather modest. Still, at $\lambda = 4867$ nm the mode has a top near-field enhancement of 55, as these weights are magnified by the factor $1/(0.5 - \chi_2)$, which is huge for the corresponding eigenvalue. The rest of the eigenmodes have the near-field enhancement maxima of 450 for the third eigenmode, of 180 for the fifth, and of 65 for the seventh dimer eigenmode at their corresponding resonance wavelengths. All these field enhancements are much larger than the enhancement of a single nanosphere.

B. Metallic nanosphere and spherical dimer in transverse polarization field

In contrast to the behavior in parallel field the LSPRs present different characteristics in transverse (field) polarization. The far-field spectrum presented in Fig. 2b shows similar spectrum for both types of NPs. The dimer resonance gets slightly smaller and slightly blue-shifted with respect to the resonance of a sphere⁴⁶. This can be also seen from Table I. Also the eigenmodes of the dimer are either hybrids of the sphere modes or proper dimer modes which are localized at the junction. These eigenmodes can be inspected comparatively to those of the sphere in the Supplementary Information. Conversely to the hybridization along the symmetry axis, in the transverse field a symmetric (even) combination of the sphere dipole modes leads to a bright dimer hybrid mode. In addition to that there is no charge accumulation at the junction with no additional near-field enhancement with respect to the sphere. The field enhancement for sphere and dimer are plotted in Fig. 4, where only the z -dependence is represented. Due to the surface parameterization, the near-field enhancement of the sphere shown in Fig. 4a does not appear to look similar to the field enhancement depicted in Fig. 1 even though they represent the same field. In Fig. 4 the field components \mathbf{E}_n , $\mathbf{E}_{t,z}$, and $\mathbf{E}_{t,\phi}$ have also a ϕ -dependence as follows. \mathbf{E}_n and $\mathbf{E}_{t,z}$ acquire the factor $\cos(\phi)$ while $\mathbf{E}_{t,\phi}$ has an additional $\sin(\phi)$ as a factor. At the extremities of the

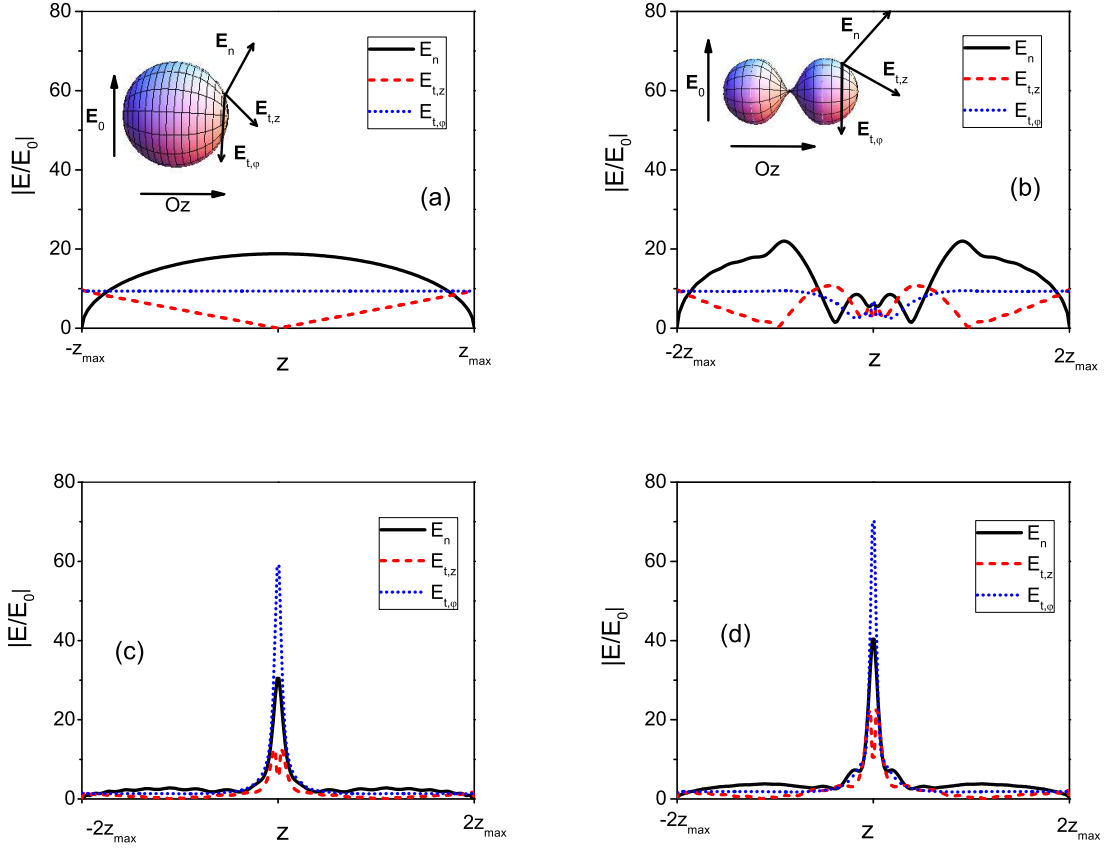


FIG. 4: The z -dependence of the near-field enhancement in transverse field for (a) the nanosphere at $\lambda = 529$ nm, (b) the dimer at $\lambda = 527.8$ nm, (c) the dimer at $\lambda = 494.5$ nm, and (d) also the dimer at $\lambda = 486.3$ nm. The normal component of the enhancement \mathbf{E}_n is plotted by black solid line, the first tangent component $\mathbf{E}_{t,z}$ by red dashed line, and the second tangent component $\mathbf{E}_{t,\phi}$ by blue dotted line. The field components \mathbf{E}_n and $\mathbf{E}_{t,z}$ have an additional multiplicative factor $\cos(\phi)$ while the component $\mathbf{E}_{t,\phi}$ has the factor $\sin(\phi)$. The insets of (a) and (b) show schematically all three components of the near-field for the sphere and for the dimer, respectively.

dimer and of the sphere the near-field enhancements of the hybrid dipoles and of the sphere dipole, respectively are equal, while they differ significantly at the junction region (Figs. 4a and 4b). The large near-field enhancement comes from the proper dimer eigenmodes that are basically dark in the far-field (Figs. 4c and 4d and Table I) but have enhancements of 65 and 75, respectively at the junction (Figs. 4c and 4d and Table I). Thus these two proper eigenmodes act as merely evanescent modes.

TABLE II: The most representative eigenmodes, their plasmon resonance wavelengths, and their weights w_k and n_k for a prolate spheroid and a nanorod with an aspect ratio of 5 : 1. The field is parallel to the symmetry axis ($\mathbf{E}_0 \parallel \mathbf{Oz}$ and $m = 0$).

spheroid					nanorod				
k	χ_k	$\lambda_k(\text{nm})$	w_k	n_k	k	χ_k	$\lambda_k(\text{nm})$	w_k	n_k
$m = 0$					$m = 0$				
1	0.5	∞	0.0	0.0	1	0.5	∞	0.0	0.0
2	0.44418	884.8	1	1.08	2	0.4481	909.5	0.9	1.17
					3	0.280		0.059	0.616
					4	0.174		0.019	-0.425
					5	0.121		0.014	-0.394
					6	0.098		0.009	0.327

C. Nanorod versus prolate spheroid in parallel field

For more than a decade a large number of wet chemistry methods have been developed for synthesis of metal NPs in a wide range of shapes and sizes⁵⁵. Of great interest are metallic nanorods due to the flexibility of controlling their aspect ratio, hence controlling their spectral response over the entire range of visible spectrum as well as in the near infrared. In general, larger aspect ratio implies larger eigenvalues and larger plasmon resonance wavelengths⁴⁶. Commonly, metallic nanorods have been modeled as prolate spheroids due to their spectral response, which can be modeled analytically and, as it turns out, is quite close to the spectral response of a nanorod. Here I consider cylindrical nanorods capped with half-spheres and prolate spheroids with the same aspect ratio like those of the nanorods. The same type of parameterization $\{x, y, z\} = \{g(z) \cos \phi, g(z) \sin \phi, z\}$ is used for spheroids and nanorods. The spheroids are defined by a function $g(z)$ of the form $g(z) = \sqrt{1 - z^2/z_{max}^2}$, where the aspect ratio is $z_{max} : 1$. In a similar manner one can also define the nanorod shape with the same aspect ratio. In numerical calculations a 5 : 1 aspect ratio is used. Table II presents the representative eigenmodes for the both types of NPs in parallel field polarization. Their far-field spectrum is presented in Fig. 5a. The second largest eigenvalue χ_2 gives the main plasmon response in both cases and the difference appears only at the

third digit. Furthermore, its weights w_2 and n_2 are also quite similar. However, Figs. 5b and 5c show that the near-field enhancement at the ends of the prolate spheroid is almost four times larger than the near-field at the ends of the nanorod (202 versus 56). The large difference in the near-field enhancement comes from the corresponding eigenfunction $u_2(z)$, which gives the spatial dependence of the field enhancement. The eigenfunction u_2 is affected at its maximum by the curvature at the ends, where the spheroid has a different curvature from that of the nanorod. Hence this result suggests that increasing the near-field enhancement requires local changes of shape in the region where the eigenfunction $u_k(z)$ reaches its absolute value maximum .

IV. CONCLUSIONS

In this work I present a powerful and intuitive technique that relates directly the near-field enhancement factor to the eigenvalues and eigenvectors associated with the BIE method. Similarly to the far-field, the near-field is expressed as a sum over the eigenmodes of the BIE operator. This property offers a general explanation of the spectral shift between the far- and near-field maxima. The current method allows fast identification of near-field hot spots just by inspecting the eigenfunctions u_k of the BIE operator and v_k of its adjoint. The normal component of the near-field enhancement peaks in the regions where the absolute value of u_k attains its maxima. Moreover the maxima of the tangent component of the near-field enhancement are found in the regions with fast variations of v_k . Although v_k is smoothed-down through Eq. (9), one can detect fast variations of v_k by looking for fast variations of u_k . In addition to that, Eq. 9 provides a physical meaning to v_k as the electric potential generated by the charge distribution u_k .

The procedure is applied to several types of NPs which exhibit large near-field enhancement. The analysis of these examples shows the strength of the current method. The first example is the dimer of nearly touching spheres. The dimer eigenmodes are either hybrids of the spherical eigenmodes or proper dimer eigenmodes. The hybrid eigenmodes exhibit charge build-up at the junction only in the parallel field polarization. The proper dimer eigenmodes, on the other hand, show strongly localized behavior at the junction in both polarizations. Thus the large near-field enhancement occurs via the huge charge accumulation and the fast potential change at the dimer junction. The second example treats the com-

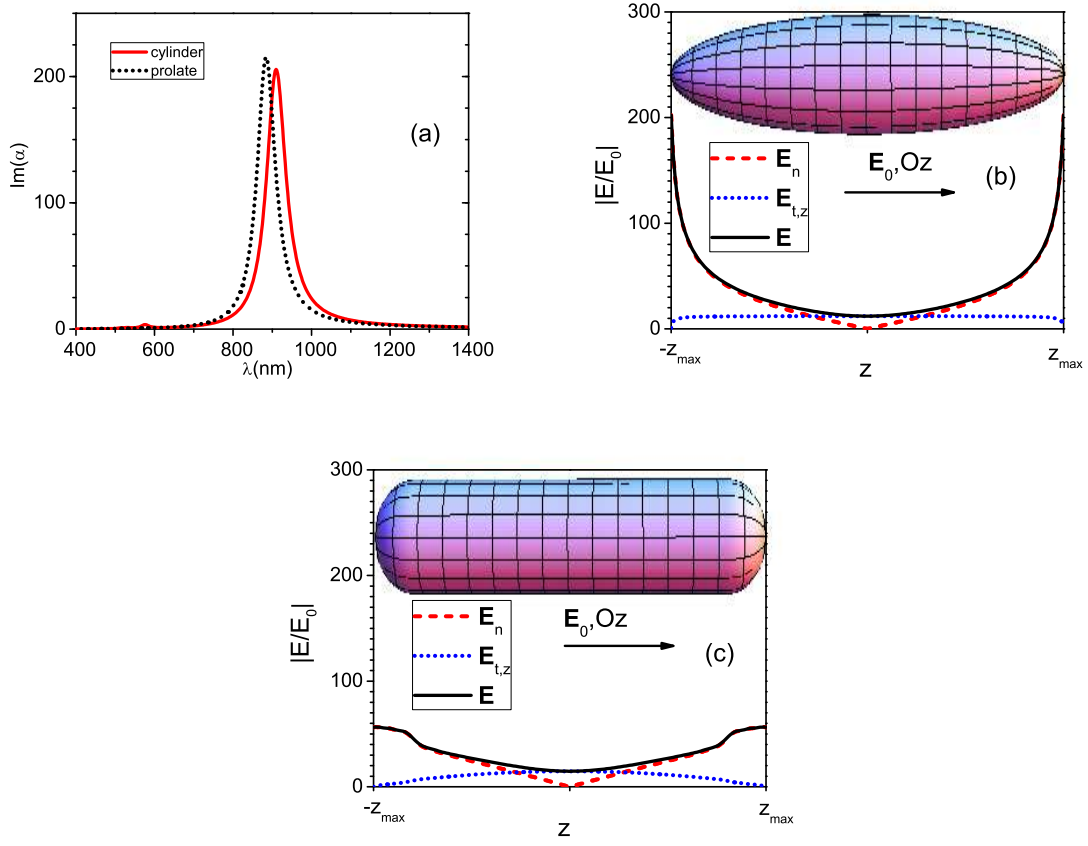


FIG. 5: (a) The far-field spectral behavior of a prolate spheroid (black dotted line) and of a nanorod (red solid line) of the same aspect ratio 5 : 1 in parallel field; the near-field enhancement of (b) the prolate spheroid at $\lambda = 884.8$ nm, and (c) of the nanorod at $\lambda = 909.5$ nm in the $x - z$ plane. The normal component of the enhancement \mathbf{E}_n is plotted by red dashed line, the tangent component $\mathbf{E}_{t,z}$ by blue dotted line, and the total enhancement \mathbf{E} by black solid line. Due to the parallel field polarization all three fields have axial symmetry.

parative near-field behavior of a nanorod and of a prolate spheroid of the same aspect ratio. These types of nanoparticles have similar far-field spectra but the near-field enhancement of the spheroid is almost four times higher at the field-oriented extremities of the nanoparticle. The latter clarifies that, in order to improve the near-field factor, one must bring targeted local corrections to the geometry by focusing on the regions where the absolute value of u_k reaches its maximum. The current methodology can be easily extended to more complex systems like assemblies of NPs.

Acknowledgments

This work has been supported by the Sectorial Operational Programme Human Resources Development, financed from the European Social Fund and by the Romanian Government under the contract number POSDRU/89/1.5/S/63700.

- * Electronic address: titus.sandu@imt.ro
- ¹ S. A. Maier, *Plasmonics: Fundamentals and Applications* (Springer, 2007).
 - ² K. M. Mayer and J. H. Hafner, *Chem. Rev.* **111**, 3828 (2011).
 - ³ S. Lal, S. Link, and N. J. Halas, *Nat. Photonics* **1**, 641 (2007).
 - ⁴ N. Engheta, *Science* **317**, 641 (2007).
 - ⁵ H. A. Atwater and A. Polman, *Nat. Mater.* **9**, 205 (2010).
 - ⁶ J. J. Mock, M. Barbic, D. R. Smith, D. A. Schultz, and S. Schultz, *J. Chem. Phys.* **116**, 6755 (2002).
 - ⁷ F. Tam, G. P. Goodrich, B. R. Johnson, and N. J. Halas, *Nano Lett.* **7**, 496 (2007).
 - ⁸ M. Danckwerts and L. Novotny, *Phys. Rev. Lett.* **98**, 026104 (2007).
 - ⁹ S. Kim, J. Jin, Y. Kim, I. Park, Y. Kim, and S. Kim, *Nature* **453**, 757 (2008).
 - ¹⁰ A. Kinkhabwala, Z. Yu, S. Fan, Y. Avlasevich, K. Müllen, and W. E. Moerner, *Nature Photonics* **3**, 654 (2009).
 - ¹¹ S. Nie and S. R. Emory, *Science* **275**, 1102 (1997).
 - ¹² J. Kneipp, H. Kneipp, and K. Kneipp, *Chem. Soc. Rev.* **37**, 1052 (2008).
 - ¹³ L. Rodriguez-Lorenzo, R. A. Alvarez-Puebla, I. Pastoriza-Santos, S. Mazzucco, O. S. and M. Kociak, L. M. Liz-Marzan, and F. J. G. de Abajo, *J. Am. Chem. Soc.* **131**, 4616 (2009).
 - ¹⁴ F. Le, D. W. Brandl, Y. A. Urzhumov, H. Wang, J. Kundu, N. J. Halas, J. Aizpurua, and P. Nordlander, *ACS Nano* **2**, 707 (2008).
 - ¹⁵ F. Neubrech, A. Pucci, T. W. Cornelius, S. Karim, A. García-Etxarri, and J. Aizpurua, *Phys. Rev. Lett.* **101**, 157403 (2008).
 - ¹⁶ R. Adato, A. A. Yanik, J. J. Amsden, D. L. Kaplan, F. G. Omenetto, M. K. Hong, S. Erramilli, and H. Altug, *Proc. Nat. Acad. Sci.* **106**, 19227 (2009).
 - ¹⁷ C. Oubre and P. Nordlander, *J. Phys. Chem. B* **108**, 17740 (2004).

- ¹⁸ B. T. Draine and P. J. Flatau, *J. Opt. Soc. Am. A* **11**, 1491 (1994).
- ¹⁹ F. J. G. de Abajo and A. Howie, *Phys. Rev. B* **65**, 115418 (2002).
- ²⁰ U. Hohenester and J. Krenn, *Phys. Rev. B* **72**, 195429 (2005).
- ²¹ E. Prodan, C. Radloff, N. J. Halas, and P. Nordlander, *Science* **302**, 419 (2003).
- ²² D. R. Fredkin and I. D. Mayergoyz, *Phys. Rev. Lett.* **91**, 253902 (2003).
- ²³ O. D. Kellogg, *Foundations of Potential Theory* (Springer, 1929).
- ²⁴ M. Putinar, D. Khavison, and H. S. Shapiro, *Arch. Rational Mech. Appl.* **185**, 143 (2007).
- ²⁵ I. D. Mayergoyz, D. R. Fredkin, and Z. Zhang, *Phys. Rev. B* **72**, 155412 (2005).
- ²⁶ T. G. Pedersen, T. S. J. Jung, and K. Pedersen, *Optics Lett.* **36**, 713 (2011).
- ²⁷ T. Sandu, D. Vrinceanu, and E. Gheorghiu, *Phys. Rev. E* **81**, 021913 (2010).
- ²⁸ T. J. Davis, K. C. Vernon, and D. E. Gomez, *Phys. Rev. B* **79**, 155423 (2009).
- ²⁹ D. W. Brandl, N. A. Mirin, and P. Nordlander, *J. Phys. Chem. B* **110**, 12302 (2006).
- ³⁰ W. Zhang, B. Gallinet, and O. J. F. Martin, *Phys. Rev. B* **81**, 233407 (2010).
- ³¹ D. E. Gomez, K. C. Vernon, and T. J. Davis, *Phys. Rev. B* **81**, 075414 (2010).
- ³² T. J. Davis, D. E. Gomez, and K. C. Vernon, *Nano Lett.* **10**, 2618 (2010).
- ³³ C. Noguez, *J. Phys. Chem. C* **111**, 3806 (2007).
- ³⁴ L. Novotny, R. X. Bian, and X. S. Xie, *Phys. Rev. Lett.* **79**, 645 (1997).
- ³⁵ T. Atay, J. H. Songa, and A. V. Nurmikko, *Nano Lett.* **4**, 1627 (2010).
- ³⁶ W. Rechberger, A. Hohenau, A. Leitner, J. R. Krenn, B. Lamprecht, and F. R. Aussenegg, *Opt. Commun.* **220**, 137 (2003).
- ³⁷ K.-H. Su, Q.-H. Wei, X. Zhang, J. J. Mock, D. R. Smith, and S. Schultz, *Nano Lett.* **3**, 1087 (2003).
- ³⁸ I. Romero, J. Aizpurua, G. W. Bryant, and F. J. G. de Abajo, *Optics Express* **14**, 9988 (2006).
- ³⁹ T. J. Davis, D. E. Gomez, and K. C. Vernon, *Phys. Rev. B* **82**, 205434 (2010).
- ⁴⁰ J. Zuloaga and P. Nordlander, *Nano Lett.* **11**, 1280 (2011).
- ⁴¹ F. J. G. de Abajo, *J. Phys. Chem. C* **112**, 17983 (2008).
- ⁴² J. Zuloaga, E. Prodan, and P. Nordlander, *Nano Lett.* **9**, 887 (2009).
- ⁴³ J. Zuloaga, E. Prodan, and P. Nordlander, *ACS Nano* **4**, 5269 (2010).
- ⁴⁴ C. David and F. J. G. de Abajo, *J. Phys. Chem. C* **115**, 19470 (2011).
- ⁴⁵ F. Ouyang and M. Isaacson, *Philos. Mag. B* **60**, 481 (1989).
- ⁴⁶ T. Sandu, D. Vrinceanu, and E. Gheorghiu, *Plasmonics* **6**, 407 (2011).

- ⁴⁷ P. Moon and D. E. Spencer, *Field Theory Handbook, Including Coordinate Systems, Differential Equations, and Their Solutions* (Springer-Verlag, New York, 1988), 2nd ed.
- ⁴⁸ G. W. Bryant, F. J. G. de Abajo, and J. Aizpurua, *Nano Lett.* **8**, 631 (2008).
- ⁴⁹ B. M. Ross and L. P. Lee, *Opt. Lett.* **34**, 896 (2009).
- ⁵⁰ J. Chen, P. Albella, Z. Pirzadeh, P. Alonso-Gonzalez, F. Huth, S. Bonetti, V. Bonanni, J. Akerman, J. Nogues, P. Vavassori, et al., *Small* **7**, 2341 (2011).
- ⁵¹ R. Alvarez-Puebla, L. M. Liz-Marzan, and F. J. G. de Abajo, *J. Phys. Chem. Lett.* **1**, 2428 (2010).
- ⁵² K. C. Vernon, A. M. Funston, C. Novo, D. E. Gomez, P. Mulvaney, and T. J. Davis, *Nano Lett.* **10**, 2080 (2010).
- ⁵³ V. V. Klimov and D. V. Guzatov, *Appl. Phys. A* **89**, 305 (2007).
- ⁵⁴ V. V. Klimov and D. V. Guzatov, *Phys. Rev. B* **75**, 024303 (2007).
- ⁵⁵ T. W. Odom and C. L. Nehl, *ACS Nano* **2**, 612 (2008).